Structural and electronic properties of silver/silicon interfaces and implications for solar cell performance

Keith T. Butler,[1] Per Erik Vullum,[2] Astrid Marie Muggerud,[3] Enrique Cabrera,[4] and John H. Harding[1]

[1]*Department of Materials Science and Engineering, University of Sheffield, Mappin Street, Sheffield S1 3JD, UK*

[2]*SINTEF Materials and Chemistry, Høgskoleringen 5, 7465 Trondheim, Norway*

[3]*Department of Physics, Norwegian University of Science and Technology (NTNU), 7491 Trondheim, Norway*

[4]*International Solar Energy Research Center - ISC Konstanz, Rudolf-Diesel-Straße 15, D-78467 Konstanz, Germany*

We present the results of an experimental and atomistic modeling investigation of the silicon/silver (Si/Ag) interfaces found in industrial solar cells. We use small *ab initio* calculations to parametrize a new interatomic potential for the Si/Ag interaction. This interatomic potential is then validated against larger *ab initio* calculations as well as the results of previous experimental and theoretical studies of Si/Ag systems. The interatomic potential allows us to perform a large-scale search of the conformational space of Si/Ag interfaces identified from transmission electron microscopy studies. The most favorable geometries thus identified are then used as the input for more accurate *ab initio* calculations. We demonstrate that the two interfaces which we identify experimentally have significantly different geometric and electronic structures. We also demonstrate how these different structures result in significantly different Schottky barriers at the interfaces.

I. INTRODUCTION

The silicon/silver (Si/Ag) interface is of great importance in industrial solar cells, with Ag commonly used in a grid to contact the Si *n*-type emitter.[1,2] The contact resistance (R_c) of this interface can have a significant impact on the overall efficiency ($\eta\%$) of the device. Indeed, the majority of process-induced losses in industrial solar cells can be attributed to the formation of metal-semiconductor contacts.

As such, understanding and tailoring the metal-semiconductor interface is of great importance in almost all semiconductor devices. The first detailed model of this interface was developed by Schottky,[3,4] and these contacts are still known as "Schottky contacts." In this paper we demonstrate how different terminations of the Si and Ag layers result in significantly different barriers to electron transport across the interface, known as "Schottky barriers." This allows future production processes to be aimed toward preferentially forming interfaces with specific terminations in order to reduce R_c.

R_c depends exponentially on the Schottky barrier (ϕ).[5] Basic Schottky theory suggests that the barrier at the interface depends only on the bulk properties of the two materials, namely the work function of the metal and the electronegativity of the semiconductor.[3,4] Early studies suggested that the Schottky barrier height (SBH) had a weak dependence on the metal type and interface fabrication method in the case of interfaces involving covalent semiconductors.[6] This effect has often been attributed to a pinning of the Fermi level of the metal by the presence of so-called metal-induced gap states (MIGS) in the band gap of the semiconductor at the interface.[7,8] One final factor, which has been studied with respect to SBH, is the influence of the surface ionicity of the semiconductor. It has been shown theoretically that the ionic charge at the semiconductor surface has a major effect on the SBH.[9,10]

There are a number of clear examples in the literature which demonstrate that the SBH at an interface is dependent not only on the bulk properties of the materials involved but also

on the interface structure itself. The silicon carbide/titanium interface, for example, has been shown experimentally to have SBHs which depend very much on the crystal faces and surface terminations involved.[11,12] Indeed it has been demonstrated for the CoSi$_2$/Si interface that interfaces between the same planes can have different SBHs depending on the bonding pattern at the interface.[13] The dependence of SBH on interface structure has also been demonstrated and investigated theoretically.[14–16] Such effects have also been investigated using experiment and theory for the zinc oxide/nickel interface, where the important role of an interface dipole in determining SBH was suggested.[17,18]

The Si(111)/Ag interface has been the subject of much investigation for many years.[19–27] Many of these studies have tended to to concentrate on Ag thin films, investigating the geometry of Ag on variously reconstructed Si surfaces. Studies of buried interfaces annealed at temperatures over 200 °C showed none of the reconstructions typically associated with the (111) surface of Si.[28,29]

The Ag/Si interface in high-performance solar cells has also been the subject of much research. Ballif *et al.*[1,30] used high-resolution electron microscopy (HREM) and energy-dispersive spectroscopy (EDS) to investigate the interface, demonstrating the growth of pyramidal Ag crystallites into the Si wafer; furthermore they were able to demonstrate the presence of an epitaxal relationship between the Si and Ag along the {111} planes. Such pyramidal crystallites have also been identified in other metal-semiconductor interface systems, for example Cu-Si[31] and Al-Si[32] systems. Recently HREM studies of the Ag-Si system have been reported;[33] again epitaxal Si/Ag interfaces on the {111} planes have been observed, and the results of this study are used to validate our theoretical calculations.

In this paper we first develop a Tersoff-type[34] interatomic potential for modeling the interaction of Si with Ag. This potential is parametrized using *ab initio* calculations of model Si/Ag systems and the validity of the new potential

is tested against experimental data and more extensive *ab initio* calculations of Si/Ag interfaces and clusters. This is used in conjunction with an existing Tersoff potential for Si[35] and a slightly modified version of an existing embedded atom model (EAM) for Ag[36] to model the Si/Ag systems. The interfaces which we choose to model were identified experimentally in transmission electron microscopy (TEM) studies of commercial solar cells. The interatomic potential provides a much quicker route to calculating optimized geometries than DFT methods. As an example, the DFT geometry optimizations in this paper consisting of around 270 atoms took around 66 hours running on 24 processors, whereas the same system calculated using the interatomic potential optimized in around five minutes on one processor. Thus the interatomic potential allows us to explore a much wider area of conformational space to find the most favorable starting geometries. These can then be used as input for the more accurate *ab initio* simulations.

The structures generated from interatomic-potential-based calculations then serve as input for *ab initio* calculations which we use to determine the SBH of two Si/Ag interfaces observed experimentally. These calculations reveal significant differences in the SBH depending on the interfacial structure. We examine the electronic structure of the two interfaces and propose an explanation, based on the differences in bonding, for the different SBHs.

II. METHODS

A. Experimental techniques

The standard solar cell process applied for this study is based on *p*-type Czochralski-grown Si wafers of 156 × 156 mm^2 size with 3–6 Ω cm base resistivity. The initial surface has random pyramidal texturing. After an HCl/HF cleaning step, POCl$_3$ diffusion was performed leading to an emitter sheet resistance from 50 to 60 Ω/sq. HF etching was carried out to remove the P-glass and SiNx was deposited by low-frequency direct-plasma PECVD. Subsequently, the wafers were front screen printed with different commercial Ag of different generations (gen2006 and gen2008) which consist of silver particles, glass frit, solvents, and binding agents. Al paste was printed on the rear side. Finally, a co-firing step was performed in an IR-heated belt furnace. Full details of the production process are available elsewhere.[37]

Cross-section TEM samples were prepared by mechanical polishing, dimpling, and Ar ion-beam thinning. The TEM experiments were performed with a JEOL 2010F operating at 200 kV.

B. Numerical calculations

All *ab initio* density functional theory (DFT) calculations were performed using the Vienna *Ab Initio* Simulation Package (VASP).[38] In all cases we employed the PBE[39] functional with a plane wave cutoff of 450 eV and projector augmented-wave pseudopotentials,[40] relaxing the forces on all atoms to less than 10^{-5} eV/Å.

Three different geometrical models were used for DFT calculations: potential derivation, potential validation, and the final electronic structure calculation. For the DFT calculations

used for potential derivation we are interested only in the interactions between the Ag and Si atoms. In these simulations model geometries consisting of 2 slabs were performed. One slab is composed of 4 layers of Si atoms, the other of 4 layers of Ag atoms. The simulations employ periodic boundary conditions (PBCs) in all directions; thus we have 2 Si/Ag interfaces in this model. For testing the validity of the new potential we compare to DFT models which are slightly larger than those employed to derive the parameters. In this case the slabs consists of 6 layers of Si and 6 layers of Ag. This allows for a more complete description of bulk plus interface effects on the structure. Again there are 2 interfaces in each model due to PBCs. For the calculations of the electronic structures and Schottky barriers we use models with 8 layers of each material. In this case we also include a vacuum gap of 12 Å in the direction normal to the interface; this means that the model contains only one Si/Ag interface. In this model the outer 3 layers of each material are frozen to the bulk positions; in addition the outer surface atoms of Si, which are undercoordinated, are passivated with H atoms.

All interatomic-potential-based calculations of the experimentally observed interfaces were performed using the DL POLY package.[41] In all cases one slab of each material was placed in contact with the other. Both slabs are 12 layers thick; again a vacuum normal to the interface is used. The outermost 4 layers of each side were frozen during the simulations. Where interatomic potentials are compared to *ab initio* for the purposes of derivation and validation calculations the systems are set up exactly as in the *ab initio* calculation.

All supercells in this paper consist of various numbers of Si and Ag unit cells in the plane of the interface, chosen in order to minimize the effects of lattice mismatch, as illustrated in Fig. 1. In all cases the remaining lattice mismatch was accounted for by compression of the Ag. The compositions and mismatches of all cells used in this paper are presented in Table I.
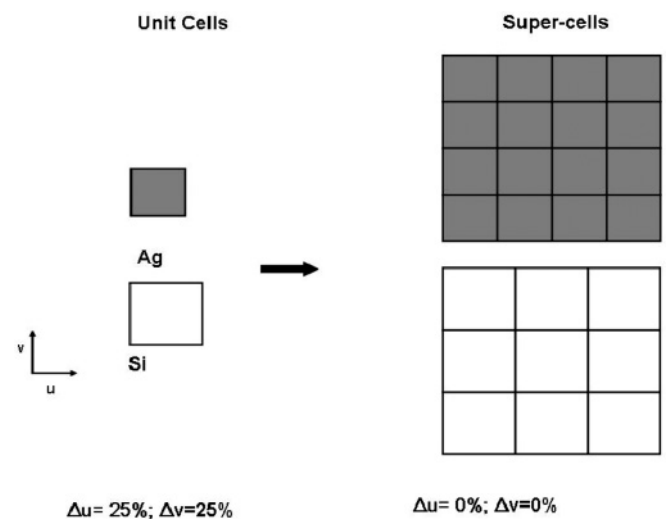

FIG. 1. Schematic illustration of the use of supercells to overcome lattice mismatch. Left: Si ($u = 7.679$ Å, $v = 7.679$ Å) and Ag ($u = 5.784$ Å, $v = 5.784$ Å) unit cells differ by 25% in u and v lattice directions. Right: Si ($\times 3$) and Ag ($\times 4$) supercells have no lattice mismatch.

TABLE I. Details of the supercells used in the three sets of calculations in this paper. In all cases the number of cells in the u vector direction by the number of cells in the v vector direction of the surface direction are given.

Interface	Ag $(u \times v)$	Si $(u \times v)$	Mismatch (u, v)
	Potential Derivation		
Ag(111)/Si(111)	4×4	3×3	0.3%, 0.3%
Ag(110)/Si(110)	4×4	3×3	0.3%, 0.3%
Ag(100)/Si(100)	3×3	2×2	11.5%, 11.5%
Ag(110)/Si(100)	3×1	4×1	4.3%, 6.1%
	Potential Validation		
Ag(110)/Si(110)	4×4	3×3	0.3%, 0.3%
Ag(110)/Si(110)	4×4	3×2	0.3%, 6.1%
	Electronic Structure		
Ag(110)/Si(110)	4×4	3×3	0.3%, 0.3%
Ag(111)/Si(111)	4×4	3×3	0.3%, 0.3%

C. Interatomic potentials

In this section we define the potential models which we have developed for the simulation on the Si/Ag interface. For Ag we have used an EAM, which has been successfully employed for modeling Ag previously.[36] For Si we used the Tersoff potential model[34] which has also been widely used for the modeling of Si and unlike the EAM can account for bond directionality as a result of the electronic structure of Si. For the interaction between the Si and Ag we again used a Tersof-type potential with additional constraints applied.

The Tersoff potential[34] is based on a simple pair potential approach. However, the attractive part of the pair potential is modified by a term which depends upon the chemical environment of the atom, thus effectively taking into account changes in bond hybridization. The interaction [$U(r_{ij})$] is calculated as

$$U(r_{ij}) = f_c(r_{ij})[f_R(r_{ij}) - \gamma_{ij} f_A(r_{ij})], \qquad (1)$$

where $f_R(r_{ij})$ and $f_A(r_{ij})$ are repulsive and attractive terms, respectively, $f_c(r_{ij})$ is a smooth cutoff function, and γ_{ij} is the bond-order term, which accounts for the local environment. The attractive and repulsive terms are calculated using exponential functions, based on the interatomic separation r_{ij} and four parameters $A_{ij}, a_{ij}, B_{ij}, b_{ij}$:

$$f_R(r_{ij}) = A_{ij} e^{-a_{ij} r_{ij}}, \quad f_A(r_{ij}) = B_{ij} e^{-b_{ij} r_{ij}}. \qquad (2)$$

The cutoff function ensures a smooth decay of the interaction and is based on two cutoff values R_{ij} and S_{ij}:

$$f_c(r_{ij}) = \begin{cases} 1 & \text{if} \quad r_{ij} < R_{ij}, \\ \frac{1}{2} + \frac{1}{2}\cos\left[\pi \frac{r_{ij} - R_{ij}}{S_{ij} - R_{ij}}\right] & \text{if} \quad R_{ij} < r_{ij} < S_{ij}, \\ 0 & \text{if} \quad r_{ij} > S_{ij}. \end{cases} \qquad (3)$$

The bond-order term depends on the angle formed between the two atoms and any third atom within the cutoff range $g(\theta_{ijk})$, the cutoff function, two atomic parameters β_i and η_i,

and two additional biatomic parameters χ_{ij} and ω_{ij}:

$$\gamma_{ij} = \chi_{ij}\left(1 + \beta_i^{\eta_i} \zeta_{ij}^{\eta_i}\right)^{\frac{-1}{2\eta_i}}, \qquad (4)$$

with

$$\zeta_{ij} = \sum_{k \neq i, j} f_C(r_{ik}) \omega_{ik} g(\theta_{ijk}), \qquad (5)$$

the θ function being defined by three further atomic parameters,

$$g(\theta_{ijk}) = 1 + \frac{c_i^2}{d_i^2} - \frac{c_i^2}{d_i^2 + (h_i - \cos\theta_{ijk})^2}. \qquad (6)$$

Furthermore, mixing parameters are defined for interactions between different atomic types, using the standard mixing rules:[42]

$$a_{ij} = (a_i + a_j)/2, \quad b_{ij} = (b_i + b_j)/2,$$
$$A_{ij} = \sqrt{A_i A_j}, \quad B_{ij} = \sqrt{B_i B_j}, \qquad (7)$$
$$R_{ij} = \sqrt{R_i R_j}, \quad S_{ij} = \sqrt{S_i S_j}. \qquad (8)$$

The biatomic parameters defining the bond order are

$$\chi_{ii} = 1, \quad \chi_{ij} = \chi_{ji},$$
$$\omega_{ii} = 1, \quad \omega_{ij} = \omega_{ji}. \qquad (9)$$

In order to ensure that the mixing rules are obeyed but that the Ag atoms do not interact through the Tersoff potential, we introduce a number of constraints to the parameters used for the Si-Ag potential. By setting $\eta_{Ag} = \frac{1}{2}$ and $\beta_{Ag} = 0$, we ensure that $\gamma_{Ag} = 1$. This means that by stipulating $A_{Ag} = B_{Ag}$ and $a_{Ag} = b_{Ag}$ during the parameter fitting process we make sure that $U_{AgAg}(r_{ij}) = 0, \forall r_{ij}$.

In addition to the Tersoff potential interaction between the Si and Ag, we include a short-range electron density term from the Si in the EAM for Ag.

III. RESULTS AND DISCUSSION

A. Experimental characterization

Figure 2 shows images from TEM investigations of the contacting interface region of the solar cells prepared according to the experimental techniques section, in which the crystalline silicon (c-Si) surface was textured along the (111) planes prior to Ag deposition. In this image the dark contrast area highlighted is an Ag crystallite embedded in the c-Si (to the right) and an amorphous layer (to the left). Such a situation is typical of Ag crystallites in solar cells. It should be noted that, in general, the fraction of c-Si where Ag crystallite contacts exist in industrial solar cells is only ~10%, the majority of the c-Si being in contact with a glass matrix.[1,37,43,44]

The diffraction pattern inset shows the alignment of the crystals. It reveals that the two structures are aligned along their (110) planes. Also, the diffraction spots are perfectly in line, demonstrating that the crystals are aligned to within the accuracy of the TEM. In addition the diffraction pattern shows that the cells are in a 3 to 4 ratio, which is what would be expected as this ratio gives almost perfectly matching lattice
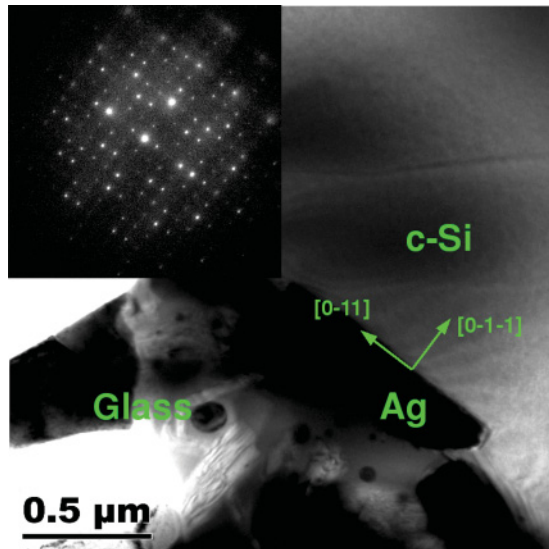
FIG. 2. (Color online) Bright-field TEM image and diffraction pattern of a Ag crystallite (dark contrast area) embedded in the c-Si matrix (area to the right).

parameters to minimize surface strain and corresponds to near-perfect epitaxial growth.

Similarly Fig. 3 shows an Ag crystallite; this time the c-Si had a polished (100) surface. The Ag is once again perfectly aligned with the c-Si; however on this occasion it is the (111) faces which are in contact with one another. The crystal orientation was determined from the diffraction pattern (inset), which again shows almost perfect alignment within the accuracy of the TEM, in a ratio of 3 to 4. These orientations are typical of the orientations found in industrial solar cells,[45] depending on the surface of the Si onto which the Ag is printed. On c-Si (100) surfaces the Ag crystallites typically grow in four-sided pyramids with (111)/(111) Si/Ag
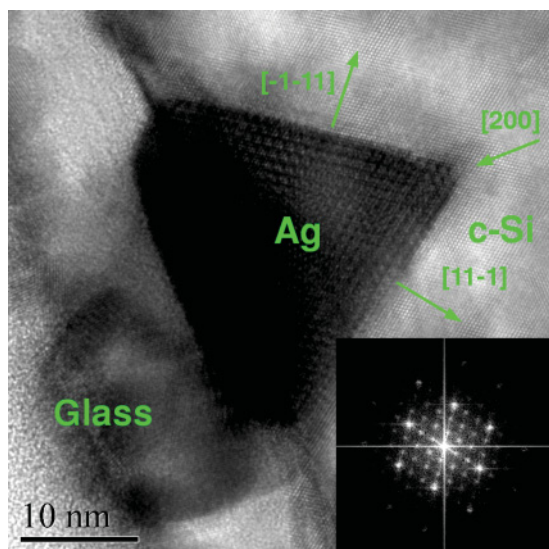

FIG. 3. (Color online) High-resolution TEM image of a Ag crystallite (triangular feature) embedded in the c-Si matrix (area to the right). The inset shows the Fourier transform of the Ag crystallite plus Si matrix.

interfaces; on c-Si which is textured to reveal the (111) surface, three-sided pyramids with a combination of (110)/(110) and (111)/(111) interfaces are typically found.[45,46]

B. Fitting the new potential

Due to the scarcity of experimental data available for fitting the Si-Ag interface potential, we have optimized the parameters to reproduce the results of *ab initio* simulations. These include the bond length and binding energy of the SiAg dimer, the geometry obtained after replacing a Ag atom in the unit cell by a Si atom, and geometry optimizing, as well as the geometries and work of separation (w_{sep}) calculated for the Si(111)//Ag(111), Si(110)//Ag(110), Si(100)//Ag(100), and Si(100)//Ag(110) interfaces. It should be pointed out that for Si/Ag interface calculations the models employed were not chosen as representative of the physical reality, but rather as references for forces acting between the species. Thus the systems were calculated as stacks of Si and Ag with no vacuum gap employed, so that each unit cell has two interfaces. The work of separation is calculated as[47]

$$w_{sep} = \frac{E_{AgSi} - (E_{Ag} + E_{Si})}{2A}, \qquad (10)$$

in which E_{AgSi} is the relaxed energy of the system with both slabs present, E_{Ag}, E_{Si} are the energies of the individual *unrelaxed* slabs, A is the interfacial area, and the factor of 2 accounts for the presence of 2 interfaces in our model systems.

In addition we have slightly altered the parameters of the Ag EAM[36] in order to reproduce the energy vs volume results from DFT calculations. This was done as we use the results of the potential-based calculations to derive structures for DFT simulations of the electronic properties of the Si-Ag interface.

The Tersoff parameters derived for Ag are given in Table II, as are the EAM parameters which have been modified.

To test the validity of the new potential we have compared to experimental data for the structure of the Ag(001) interface with the 2 × 1 reconstructed Si(001) surface, the Ag(011) interface with the 2 × 1 reconstructed Si(001) surface,[48,49] and recent HREM values for the *d* spacing of the 111 planes at the Ag(111)//Si(111) interface.[33] We also compare to higher level theoretical calculations, DFT structures of the Ag(110)//Si(110) interface and the Ag(100)//Si(110) interface (calculated with thicker slabs than used when deriving the potential; see numerical details section), as well as

TABLE II. Potential parameters derived in this work. Tersoff parameters are as in Eqs. (1)–(7) and EAM parameters are as in Ref. 36.

Tersoff		EAM	
A (eV)	99.93	α	7.689628
a (Å^{-1})	1.016	r_{eq} (Å)	2.959130
B (eV)	99.93		
b (Å^{-1})	1.016		
R (Å)	4.50		
S (Å)	4.51		
β	0		
η	0.5		

TABLE III. Comparison of the optimized geometrical properties of SiAg clusters and interfaces calculated using the new potential and those observed experimentally and calculated from DFT. All distances are in Å and angles are in degrees.

Observable	Theory	Experiment	New Potential
Ag(001)/Si(001) (2×1)			
Ag(s)-Ag(s)		2.89[a]	2.93
Ag(s)-Ag(b)3		4.09[a]	4.07
Ag(011)/Si(001) (2×1)			
Ag(s)-Ag(s)		2.89[b]	2.89
Ag(s)-Ag(s) II		4.09[b]	4.09
Ag(s)-Ag(b)2		2.80[b]	2.88
Ag(110)/Si(110)			
Ag-Si	2.66		2.75
$\angle$Ag-Si-Ag I	52.39		53.92
$\angle$Ag-Si-Ag II	120.93		119.45
Ag(100)/Si(110)			
Ag-Si	2.72		2.73
$\angle$Ag-Si-Ag I	52.18		55.91
$\angle$Ag-Si-Ag II	88.06		89.66
AgSi separations			
Ag-Si$_2$	2.63[c]		2.71
AgSi$_3$	2.56[c]		2.57
AgSi$_4$ C_{2v}	2.64[c]		2.69
AgSi$_4$ C_1	2.75[c]		2.80
AgSi$_5$ C_{2v}	2.65[c]		2.65
111 interplanar d spacings			
Ag		2.58[d]	2.40
Si		3.43[d]	3.30

[a]Reference 48.
[b]Reference 49.
[c]Reference 50.
[d]Reference 33.

TABLE IV. Interatomic separations of Si to Ag and Si (Ag) to first Si (Ag) back layer in Å.

Interface	Si-Ag	Si-Si	Ag-Ag
111	2.69	2.35	2.89
110	2.65	2.36	2.87

C. Interface structure

We now investigate the geometry and electronic structure of the two interfaces which have been identified by TEM. The initial step is to use the potential derived in the previous section to generate a starting geometry for the DFT calculations. The starting geometries are generated using the Materials Studio[51] package. The systems are then set up as described in the numerical calculations section. Using the potential we can investigate a number of important factors for setting up the DFT calculations. First we can establish a starting configuration which can be expected to give the lowest energy configuration. This is achieved in a two-step process, by varying the slab separation, followed by the x and y Cartesian coordinates of the Ag slab and relaxing the resultant geometry to find the lowest energy minimum. This required 150 separate
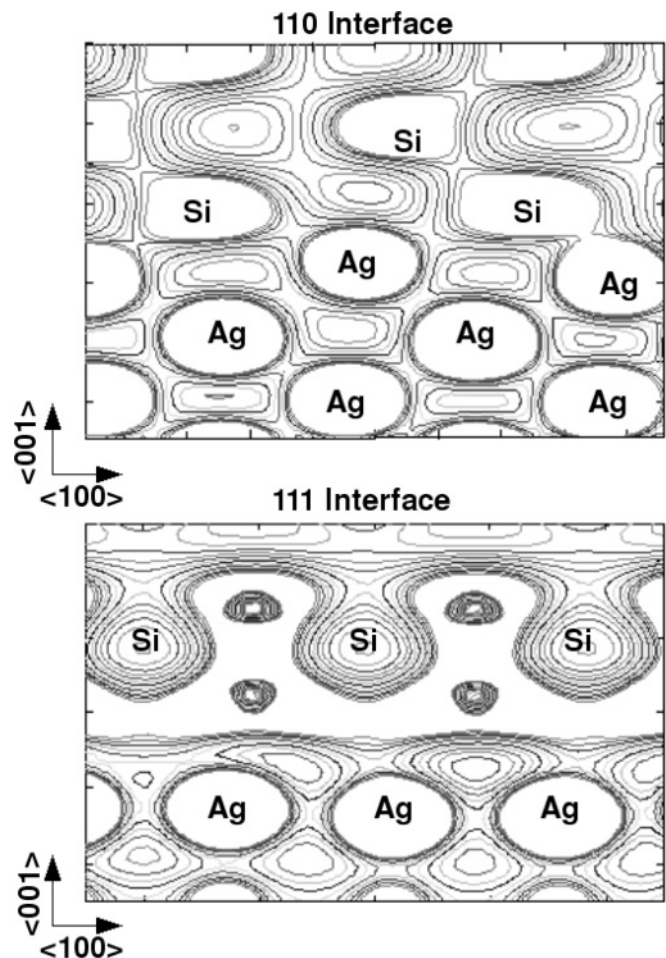

FIG. 4. Charge distribution in the [100] cross section at the 110//110 (upper) and 111//111 (lower) Si/Ag interfaces. Charge density contours from 0.001 to 0.281 a.u.$^{-3}$ are shown.

structural details of theoretically calculated AgSi$_n$ structures taken from the literature.[50] The comparisons are presented in Table III.

All of our calculated cluster bond lengths are within 5% of the DFT values,[50] although our potential was based primarily on condensed state data. Of more interest are the comparisons to interface structures. The relaxation of the surfaces in contact with one another can be characterized by the interatomic distances at the surface as well as the interlayer distances of the surface to bulk layer atoms. These values are available experimentally for Ag surfaces in contact with the reconstructed Si(001) (2×1) surface. In all cases the values which we calculate are within 3% of the experimental values. When comparing to the DFT structures of the more realistic interface models we find the interatomic separations obtained from the potential model to be within 5% of the *ab initio* results and generally good agreement for bond angles (see Table III). Finally we also compare to recent HREM results for d spacings at the Si/Ag interface in a crystalline Si solar cell;[33] we find that our values are within 0.2 Å of the experimental values, which is within the spatial resolution of the HREM method.

geometry optimizations, which would be extremely time consuming using DFT methods. Second, we can investigate how far beyond the interface the geometrical rearrangements are manifested. This allows us to choose the smallest possible slabs for the DFT calculation, thus improving efficiency. In the case of both interfaces it was found that significant reorganization of the atomic positions compared to the ideal crystal positions (> 0.1 Å) occurred only within the first 5 Å either side of the interface.

As presented in Table IV, the interatomic distance between the Si and Ag surface atoms is slightly smaller in the 110//110 interface. In the case of the 111//111 interface there is very little distortion of the surface layer to back layer distances on either side of the interface, with both Si-Si and Ag-Ag bonds being within 0.01 Å of the ideal crystal values. In the 110//110 case, the Si-Si bond between the surface and back layer is slightly stretched relative to the perfect crystal, while the Ag-Ag bond is slightly compressed. The striking feature, however, is how little the bond lengths differ between the two interfaces. This minor difference masks a significant difference between the electronic structures of the two interfaces as we shall now show.

D. Electronic structure

Figure 4 shows the charge distribution calculated for the interfacial structures. The 111//111 interface shows little major change in the charge density at the surface compared to the bulk layers on either side. There is also very little apparent covalent-type bonding between the Si and the Ag. This interface has bonding which is rather metallic in nature, with a broad charge distribution.

In contrast to this, the 110//110 interface shows substantial charge density interactions across the interface. The Si-Ag atoms are forming a quasi-covalent bond. The reason for the major difference in the charge distributions is, we believe, due to the bonding environments at the different interfaces. At the 111//111 interface the surface Si atoms are back-bonded
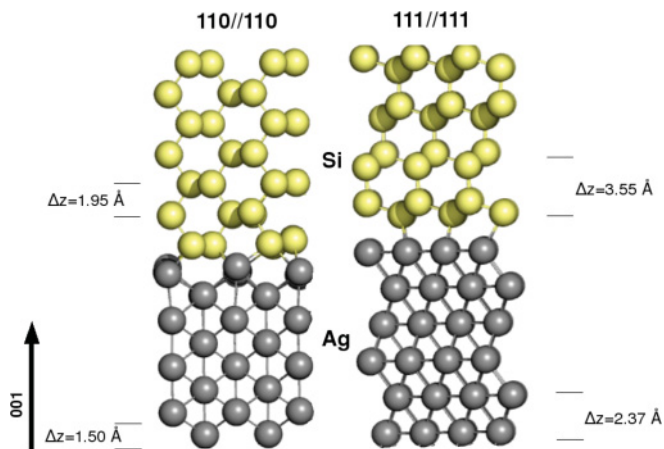

FIG. 6. (Color online) Interface geometries of the 111//111 and 110//110 Si/Ag interfaces, showing interlayer spacing along the 001 axis.

to three fully coordinated Si atoms. Thus their electronic environment is similar to that in the bulk crystal. In the 110//110 interface, however, the surface Si atoms are bonded to only one fully coordinated Si and two other interface Si atoms, perhaps resulting in bonds being formed to Ag. These differences in atomic structure affect the electronic profile of these interfaces which in turn can have a marked effect on their macroscopic electrical properties as we shall now explore.

Figure 5 shows the valence charge densities averaged in the (001) plane plotted along the (001) axis in both interfaces. Again this plot makes apparent the difference in electronic structure of the two interfaces. The reason for the more pronounced oscillations in the 111//111 charge density (Fig. 5) is that the interlayer spacing along the (001) axis is greater in this structure (Fig. 6). Returning to Fig. 5, at the 110//110 interface there is a marked decrease in the Ag charge density at the surface layer. There is also a very slight increase in the charge density at the Si surface layer. This shows an obvious charge transfer of valence electrons from Ag to Si at this interface. The 111//111 interface shows no such changes at the interface with the densities on either side being the same as their bulk values. These analyses reflect the bonding situations revealed in Fig. 4.

Figure 7 shows the averaged projected density of states (PDOS) for the layers of each Si slab closest to the Si/Ag interface. It should be noted that the sharper features in the (111) interface PDOS are most likely due to the fact that there are fewer Si atoms in each layer. While the interlayer spacing in the 110//110 interface is constant, in the 111//111 interface we have split each Si layer in the 111//111 (depicted in Fig. 6) structure into bilayers, according to their distance from the interface along the (001) axis, for the PDOS plot.

One of the most important features of the PDOS plots is the existence of states within the band gap at the surface layer Si atoms. These are the metal-induced gap states (MIGS).[7,8] The MIGS-charge neutrality level (MIGS-CNL) model,[7] in which the CNL is the energy level to which the band structure is filled in the neutral system, insists that the presence of these states seriously affects the Schottky barrier at an interface.
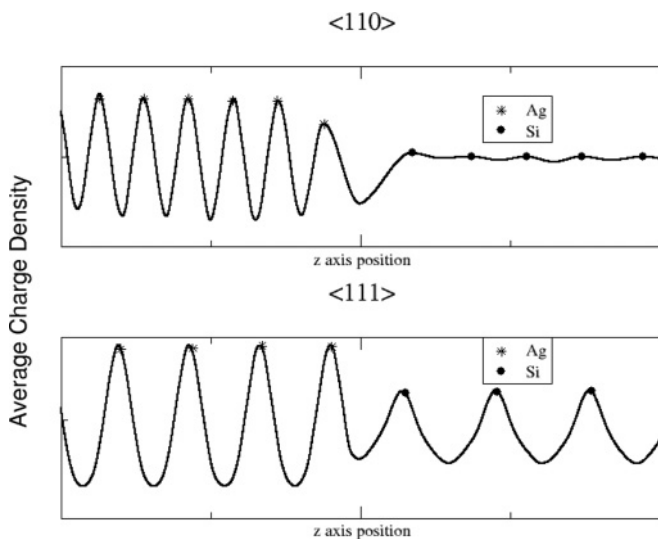

FIG. 5. Averaged, normalized charge densities along the 001 axis of the 110//110 (top) and 111//111 (bottom) interfaces. The positions of the atomic layers are indicated by a point.
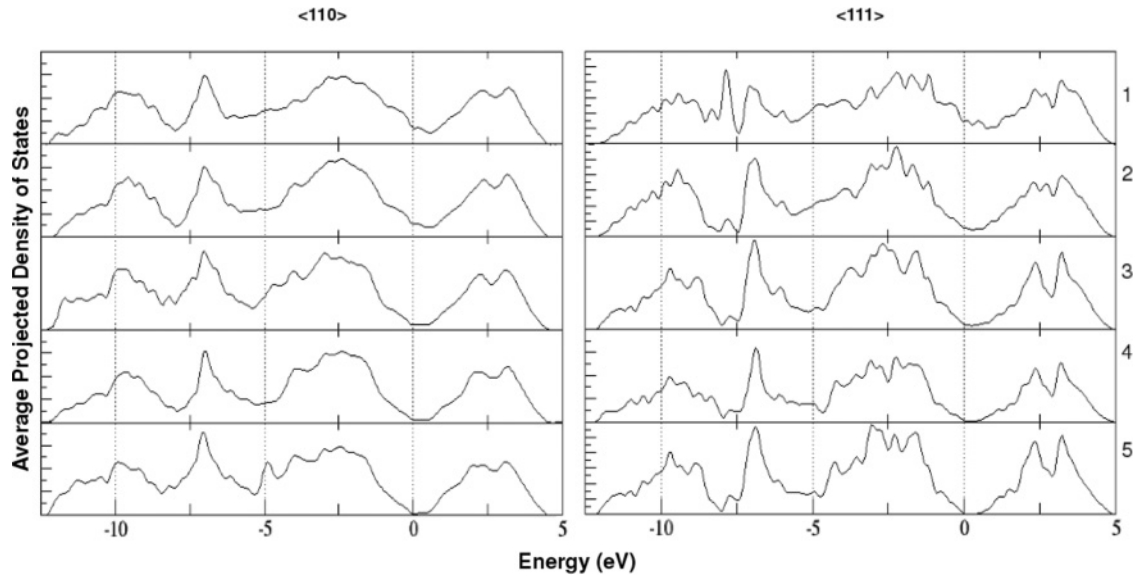
FIG. 7. Averaged projected density of states of the Si atoms in each layer moving away from the Si/Ag interface from the top down. The supercell Fermi level is set to zero.

As can be seen in the PDOS plots the MIGS in the 111//111 system decay much more rapidly away from the interface than those in the 110//110 system. In the 111//111 system the states are almost completely absent in the second layer of Si atoms, which is less than 1 Å farther from the interface than the first layer. In contrast the 110//110 still displays some MIGS in the second layer of Si atoms which are 1.95 Å farther from the interface than the surface layer. We believe that the reason for the deeper MIGS in the 110//110 system is the presence of electron density transferred from the Ag layer in the Si layer. As shown in Fig. 5 this is more prevalent in the 110//110 interface.

E. Schottky barrier height

A *p*-type Schottky barrier height (SBH) can be obtained from a supercell calculation as the difference between the Fermi level of the supercell and the valence-band top (VBT) of the bulk semiconductor region.[15,16] From this the *n*-type SBH can easily be obtained as the semiconductor band gap minus the *p*-type SBH. Of course in these calculations there are no band-bending effects, due to the absence of dopant and temperature effects. However such calculations provide insight into SBHs in the ideal limit and are useful for the comparison of different interfaces. While MIGS and classic Schottky theories insist that the SBH is a property only of the bulk materials on either side of the interface, it has been shown both theoretically and experimentally that the SBH can vary greatly depending on the local interface structure.[15–18]

Since, as can be seen in Fig. 7, the PDOSs of the Si away from the interface still display some disorder, particularly close to the VBT, we determine the VBT by fitting the valence band bottom (VBB) of bulk Si to that of the interface system and taking the VBT from the bulk DOS, as has been done previously.[15,16] The *n*-type SBH is then calculated by subtracting the *p*-type SBH from the Si band gap. In this case we use the experimental band gap, as generalized gradient approximation methods (such as the PBE functional used in this work) often seriously underestimate band gaps. The SBHs thus calculated are presented in Table V.

The SBHs for the two interfaces show a significant difference of 0.25 eV. We propose that this difference arises from the different bonding structures at the two interfaces. In the 110//110 interface there is a higher degree of covalency between the Si and Ag atoms (Fig. 4). This, in turn, results in a transfer of some electron density from Ag and Si (Fig. 5) to the interfacial region. This charge transfer means that the surface Si sites in the 110//110 system have a slightly less negative charge compared to those in the 111//111 interface.

Within a classical macroscopic model the negative charge in the semiconductor screened by its dielectric constant is neutralized by a positive charge induced in the metal layer.[10] Thus a dipole is established across the interface. This dipole results in the raising of the electrostatic potential of the semiconductor with respect to the metal. Due to the dependence of the SBH on the potential difference between the metal and semiconductor,[10,17,18] this results in an decreased SBH at the interface. This dipole in the 110//110 interface is lowered compared to that in the 111//111 interface, due to charge transfer; thus the *p*-type SBH is higher in the 110//110 interface.

TABLE V. Schottky barrier heights (ϕ) for the Si/Ag 110//110 and 111//111 systems as calculated from supercell simulations.

Interface	ϕ_p		ϕ_n	
	Calc.	Expt.	Calc.	Expt.
110//110	0.55	0.57[a]	0.55	
111//111	0.30		0.80	0.74[b]

[a]Reference 52.
[b]Reference 53.

IV. SUMMARY

We have presented a new potential for the interaction between silicon and silver based on the Tersoff functional form. The model has been parametrized to fit *ab initio* data and validated against both *ab initio* and experimental data. We have then used this potential to investigate the geometry of two Si/Ag interfaces which we have identified, by means of TEM, in industrially produced solar cells.

The geometries which we have obtained from the potential-based calculations have served as input for *ab initio* calculations of the electronic structure of the interfaces. We have calculated SBHs in good agreement with experimental values, showing that the *p*-type SBH for the 111//111 Si/Ag interface is significantly lower than that of the 110//110 interface. This reinforces the idea that the SBH is dependent not only on the bulk properties of the materials involved in an interface, but also on the local structure at the interface.

Using the calculated electronic structure we have attempted to rationalize the difference in SBH at the two interfaces. We propose that the presence of covalent bonding at the 110//110 interface results in a charge transfer into the interfacial region, leading to a reduction in the dipole across the interface caused by the negative charge on surface layer Si, which induces an image charge in the Ag. As this dipole results in the lowering of the *p*-SBH ϕ_p the reduction of the dipole can explain the higher value of ϕ_p at the 110//110 interface.

We believe that in light of these results, future production of solar cells would benefit from being tailored to form 110//110 Si/Ag contacts to transport charge generated in *n*-type Si, in order to reduce contact resistance. A small contact resistance is particularly desirable in the *n*-type Si/Ag contact, due to the fact that this contact is normally formed on the front side of the solar cell, meaning that it is desirable to have as small a layer of metal contact as possible, to allow maximum light penetration into the cell. Thus, a low contact resistance between Si and Ag is one of the primary concerns when producing solar cells to ensure good performance of the solar cell despite a small metal/semiconductor contact area. It should be noted, however, that the barriers calculated here are local barriers for Si/Ag contacts. The values do not give a global resistance for the entire cell. While the values give an indication of which interfaces are best for current transport, the incorporation of the calculated barriers into macroscopic models of the full device will be necessary to fully appreciate the implications of the results.

[1] C. Ballif, D. M. Huljić, G. Willeke, and A. Hessler-Wyser, Appl. Phys. Lett. **82**, 1878 (2003).

[2] Z. G. Li, L. Liang, and L. K. Cheng, J. Appl. Phys. **105**, 066102 (2009).

[3] W. Schottky, Z. Phys. **113**, 367 (1939).

[4] W. Schottky, Z. Phys. **118**, 539 (1942).

[5] A. Y. C. Yu, Solid-State Electron. **13**, 239 (1970).

[6] W. Monch, editor, *Electronic Structures of Metal-Semiconductor Contacts* (Jaca, Milano, 1990).

[7] V. Heine, Phys. Rev. **138**, A1689 (1965).

[8] J. Tersoff, Phys. Rev. Lett. **52**, 465 (1984).

[9] S. G. Louie, J. R. Chelikowsky, and M. L. Cohen, Phys. Rev. B **15**, 2154 (1977).

[10] C. Berthod, N. Binggeli, and A. Baldereschi, Phys. Rev. B **68**, 085323 (2003).

[11] J. R. Waldrop and R. W. Grant, Appl. Phys. Lett. **62**, 2685 (1993).

[12] J. R. Waldrop, J. Appl. Phys. **75**, 4548 (1994).

[13] P. Werner, W. Jäger, and A. Schüppen, J. Appl. Phys. **74**, 3846 (1993).

[14] J. Hoekstra and M. Kohyama, Phys. Rev. B **57**, 2334 (1998).

[15] M. Kohyama and J. Hoekstra, Phys. Rev. B **61**, 2672 (2000).

[16] S. Tanaka and M. Kohyama, Phys. Rev. B **64**, 235308 (2001).

[17] Y. F. Dong, S. J. Wang, J. W. Chai, Y. P. Feng, and A. C. H. Huan, Appl. Phys. Lett. **86**, 132103 (2005).

[18] S. Wang, Y. Dong, C. Huan, Y. Feng, and C. Ong, Mater. Sci. Eng. B **118**, 122 (2005).

[19] N. Sasaki, S. Watanabe, and M. Tsukada, Phys. Rev. Lett. **88**, 046106 (2002).

[20] Y. G. Ding, C. T. Chan, and K. M. Ho, Phys. Rev. Lett. **67**, 1454 (1991).

[21] H. M. Zhang and R. I. G. Uhrberg, Phys. Rev. B **74**, 195329 (2006).

[22] H. Hirayama, T. Komizo, T. Kawata, and K. Takayanagi, Phys. Rev. B **63**, 155413 (2001).

[23] R. I. G. Uhrberg, H. M. Zhang, T. Balasubramanian, E. Landemark, and H. W. Yeom, Phys. Rev. B **65**, 081305 (2002).

[24] H. M. Zhang, J. B. Gustafsson, and L. S. O. Johansson, Phys. Rev. B **74**, 201304 (2006).

[25] S. J. Chey, L. Huang, and J. H. Weaver, Phys. Rev. B **59**, 16033 (1999).

[26] J.-K. Zuo and J. F. Wendelken, Phys. Rev. B **56**, 3897 (1997).

[27] F.-C. Chuang, C.-H. Hsu, C.-Z. Wang, and K.-M. Ho, Phys. Rev. B **78**, 245418 (2008).

[28] H. Hong, R. D. Aburano, D.-S. Lin, H. Chen, T.-C. Chiang, P. Zschack, and E. D. Specht, Phys. Rev. Lett. **68**, 507 (1992).

[29] R. D. Aburano, H. Hong, J. M. Roesler, K. Chung, D.-S. Lin, P. Zschack, H. Chen, and T.-C. Chiang, Phys. Rev. B **52**, 1839 (1995).

[30] C. Ballif, D. Huijic, A. Hessler-Wyser, and G. Willeke, in Photovoltaic Specialists Conference, 2002, Conference Record of the Twenty-Ninth IEEE, pp. 360–363.

[31] Y.-L. Kuo, J.-J. Huang, S.-T. Lin, C. Lee, and W.-H. Lee, Mater. Chem. Phys. **80**, 690 (2003).

[32]H.-C. Fang, C.-P. Liu, H.-S. Chung, and C.-L. Huang, Microsc. Microanal. **16**, 1340 (2010).

[33]M.-I. Jeong, S.-E. Park, D.-H. Kim, J.-S. Lee, Y.-P. Park, K.-S. Ahn, and C.-J. Choi, J. Electrochem. Soc. **157**, H934 (2010).

[34]J. Tersoff, Phys. Rev. Lett. **56**, 632 (1986).

[35]J. Tersoff, Phys. Rev. B **39**, 5566 (1989).

[36]X. W. Zhou, H. N. G. Wadley, R. A. Johnson, D. J. Larson, N. Tabat, A. Cerezo, A. K. Petford-Long, G. D. W. Smith, P. H. Clifton, R. L. Martens, and T. F. Kelly, Acta Mater. **49**, 4005 (2001).

[37]G. Schubert, Ph.D. thesis, Universitat Konstanz, 2006.

[38]G. Kresse and J. Furthmuller, Phys. Rev. B **54**, 11169 (1996).

[39]J. P. Perdew, K. Burke, and M. Ernzerhof, Phys. Rev. Lett. **77**, 3865 (1996).

[40]G. Kresse and D. Joubert, Phys. Rev. B **59**, 1758 (1999).

[41]W. Smith and T. R. Forester, J. Mol. Graphics **14**, 136 (1996).

[42]M. P. Allen and D. J. Tildesley, editors, *Computer Simulation of Liquids* (Clarendon Press, Oxford, 1987).

[43]K.-K. Hong, S.-B. Cho, J. S. You, J.-W. Jeong, S.-M. Bea, and J.-Y. Huh, Solar Energy Materials and Solar Cells **93**, 898 (2009), 17th International Photovoltaic Science and Engineering Conference.

[44]S. Kontermann, M. Hrteis, M. Kasemann, A. Grohe, R. Preu, E. Pink, and T. Trupke, Solar Energy Materials and Solar Cells **93**, 1630 (2009).

[45]S. Kontermann, Ph.D. thesis, Universitat Konstanz, 2009.

[46]D. Pysch, A. Mette, A. Filipovic, and S. W. Glunz, Prog. Photovoltaics **17**, 101 (2009).

[47]M. W. Finnis, J. Phys. Condens. Matter **8**, 5811 (1996).

[48]Y. W. Kim, N. G. Park, W. S. Cho, K. H. Chae, C. N. Whang, K. S. Kim, S. S. Kim, and D. S. Choi, Surf. Sci. **396**, 295 (1998).

[49]W. S. Cho, J. Y. Kim, N. G. Park, K. H. Chae, Y. W. Kim, S. S. Kim, D. S. Choi, and C. N. Whang, Surf. Sci. **439**, L792 (1999).

[50]P.-F. Zhang, J.-G. Han, and Q.-R. Pu, J. Mol. Struct., Theochem. **635**, 25 (2003).

[51]Materials Studio (Accelrys, Accelrys Software, Inc., 2001–2007).

[52]J. Garramone, J. Abel, I. Sitnitsky, and V. LaBella, J. Vac. Sci. Technol. A **28**, 643 (2010).

[53]R. F. Schmitsdorf, T. U. Kampen, and W. Monch, Surf. Sci. **324**, 249 (1995).